

Supporting Information

Molecular engineering low-surface energy membranes by grafting perfluoro-tert-butoxy chains containing fluorosilica aerogels

Vicki Man-Wai Yim^{a, 1}, See-Wing Lo^{b, 1}, Bhaskar Jyoti Deka^a, Jiabin Guo^a, Jehad A. Kharraz^a, István T. Horváth^{b*}, and Alicia Kyoungjin An^{a*}

^a School of Energy and Environment, City University of Hong Kong, Tat Chee Avenue, Kowloon, Hong Kong, China

^b Department of Chemistry, City University of Hong Kong, Tat Chee Avenue, Kowloon, Hong Kong, China

*Corresponding authors: István T. Horváth istvan.t.horvath@cityu.edu.hk and Alicia Kyoungjin An alicia.kjan@cityu.edu.hk

¹ These authors contributed equally to this work.

Supporting Information includes

Number of pages: S18

Number of Figures: 10

Number of Tables: 4

Number of Method: 1

Number of Videos: 1

Figure S1. Schematic of membrane fabrication by electrospraying technique.....	S2
Figure S2. Flow diagram of the experimental DCMD process.....	S2
Figure S3. The green perfluoroalkyl groups withdrew the electrons from the attaching carbon, the longer the perfluoroalkyl chains, the stronger the electron-withdrawing effect. The blue carbon in the linear long perfluoroalkyl chain is more electron deficient than black carbon in the short branched perfluoroalkyl groups, since the black carbon has an alkyl chain R which is electron donating.....	S3
Figure S4. XPS analysis of the fluorinated aerogel-coated membrane surfaces: (a) F₁-SiG50 , (b) F₂-SiG50 , and (c) F₃-SiG50	S4
Figure S5. Water abrasion test of F₁-SiG100	S5
Figure S6. Photos of membranes' in-air CAs with water, 7% NaCl solution, and 7% NaCl with 0.1 mM SDS solution, and under-water oil CAs with cooking oil.....	S6
Figure S7. Time-dependent UV-vis spectra of F₁-SiG100 's oil-water separation permeate.	S7
Figure S8. Photos of the (A) feed side holding the dyed water, and (B) the permeate side of the F₁-SiG100 membrane after oil-water separation testing.....	S8
Figure S9. The re-entrant structures of the modified membranes.....	S9
Figure S10. DCMD performances of the fluorinated aerogel membranes with stepwise SDS addition (0.1 ~ 0.5 mM) in 3.5% NaCl solution: (a) F₁-SiG25 , (b) F₁-SiG50 , (c) F₁-SiG100 , (d) F₂-SiG25 , (e) F₂-SiG50 , (f) F₃-SiG25 , (g) F₃-SiG50 , and (h) C-PVDF membranes. The initial fluxes were observed as 24.29 ± 0.31 , 23.94 ± 0.52 , 24.25 ± 0.40 , 23.89 ± 0.27 , 24.12 ± 0.33 , 24.39 ± 0.51 , 23.76 ± 0.42 and 26.47 ± 0.47 L m ⁻² h ⁻¹ , respectively	S10
Table S1. Surface tension of solvents used in the study.....	S11
Table S2. The BET surface area, porosity and surface free energy of membranes.....	S12
Table S3. Oil/water separation measurements and the oil adsorption of F₁-SiG100 membrane.....	S13
Table S4. Comparison of DCMD performance against low surface tension feed.	S14
Method S1. Working principle, mathematical models and detailed procedure of measuring membranes surface roughness using optical surface profiler (Wyko NT9300, Veeco).....	S15
Video S1. Superoliphilicity of F₁-SiG100 by dropping chloroform.....	S17

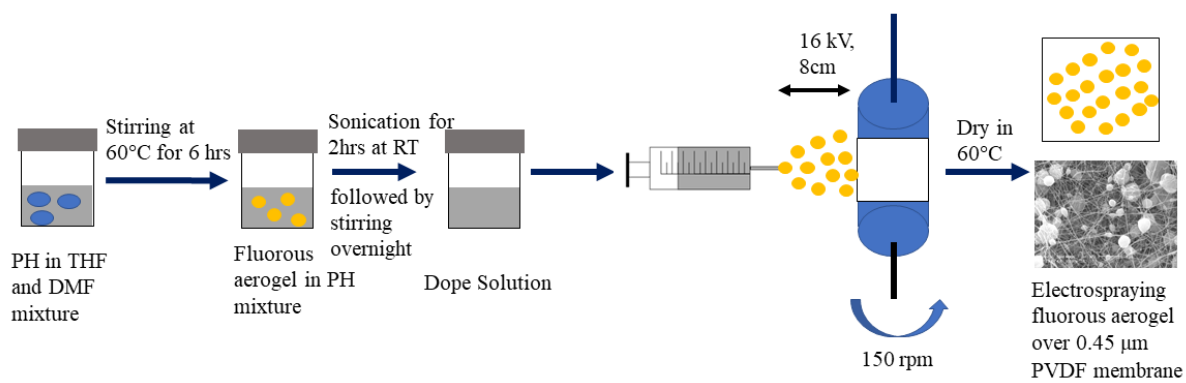


Figure S1. Schematic of membrane fabrication by electrospaying technique.

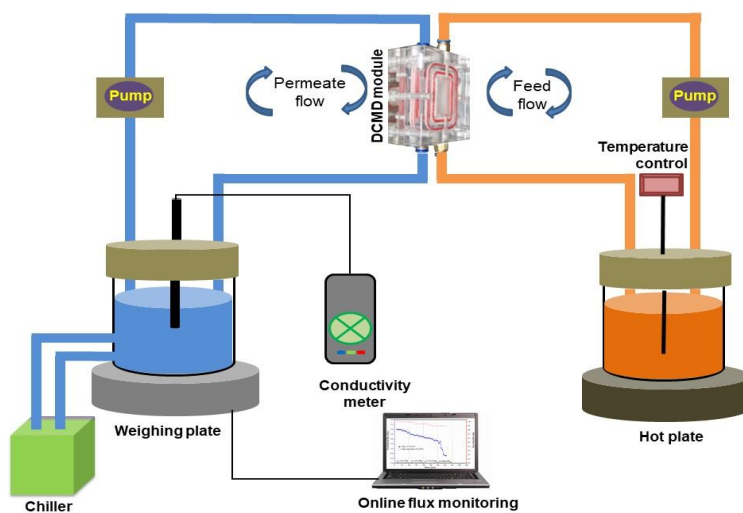
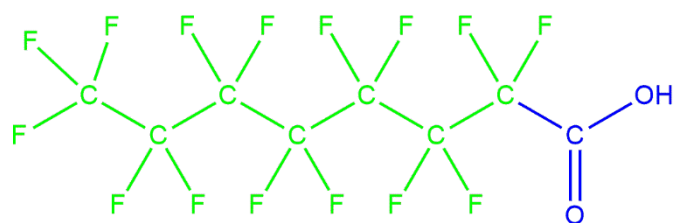
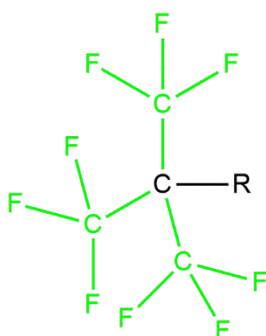


Figure S2. Flow diagram of the experimental DCMD process.



Linear long perfluoroalkyl chain



Short branched perfluoroalkyl group

Figure S3. The green perfluoroalkyl groups withdrew the electrons from the attaching carbon, the longer the perfluoroalkyl chains, the stronger the electron-withdrawing effect. The blue carbon in the linear long perfluoroalkyl chain is more electron deficient than black carbon in the short branched perfluoroalkyl groups, since the black carbon has an alkyl chain R which is electron donating

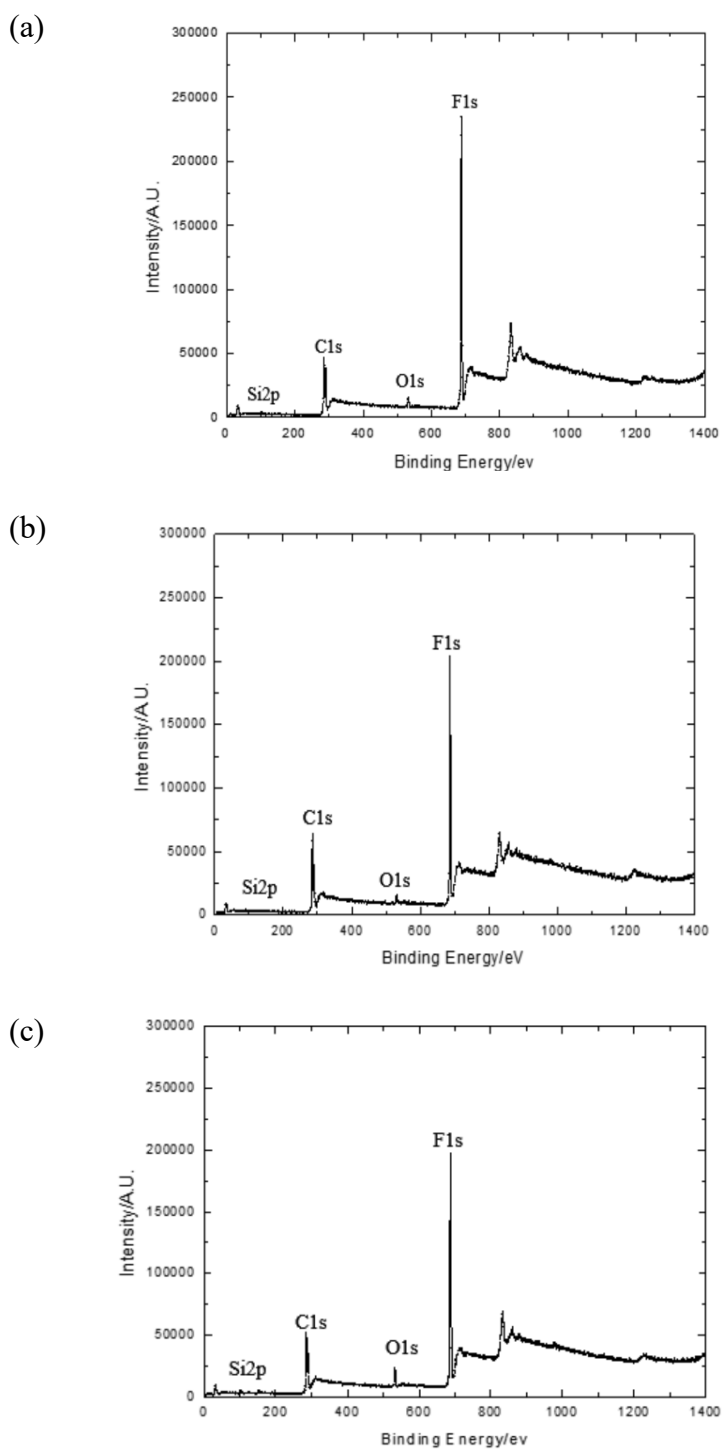


Figure S4. XPS analysis of the fluorinated aerogel-coated membrane surfaces: (a) **F₁-SiG50**, (b) **F₂-SiG50**, and (c) **F₃-SiG50**.

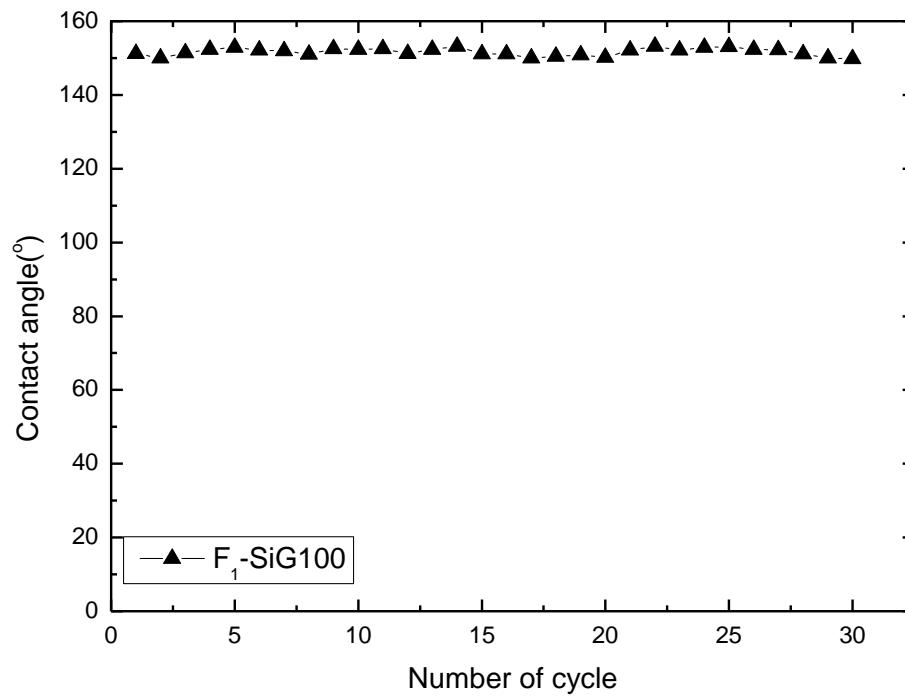


Figure S5. Water abrasion test of F₁-SiG100.

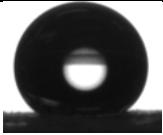
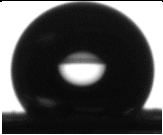
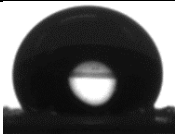

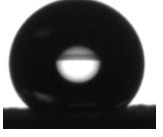
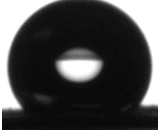
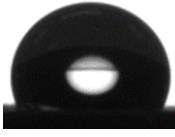
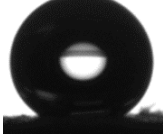
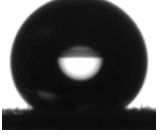
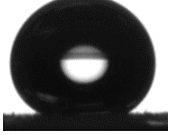
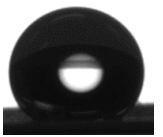
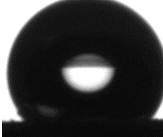
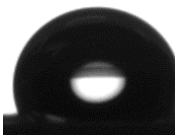
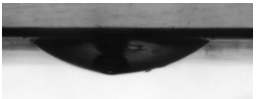
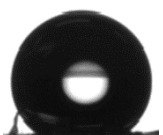

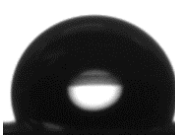
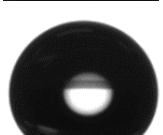

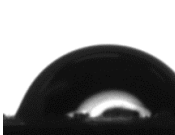
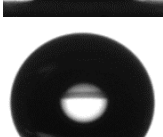
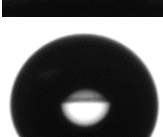
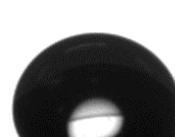
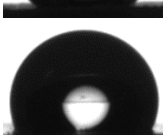

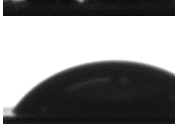
	In-air CA			Under-water CA
	Water	7% NaCl solution	7% NaCl and 0.1 mM SDS solution	Cooking oil
F ₁ -SiG25				
F ₁ -SiG50				
F ₁ -SiG100				
F ₂ -SiG25				
F ₂ -SiG50				
F ₃ -SiG25				
F ₃ -SiG50				
PVDF				

Figure S6. Photos of membranes' in-air CAs with water, 7% NaCl solution, and 7% NaCl with 0.1 mM SDS solution, and under-water oil CAs with cooking oil.

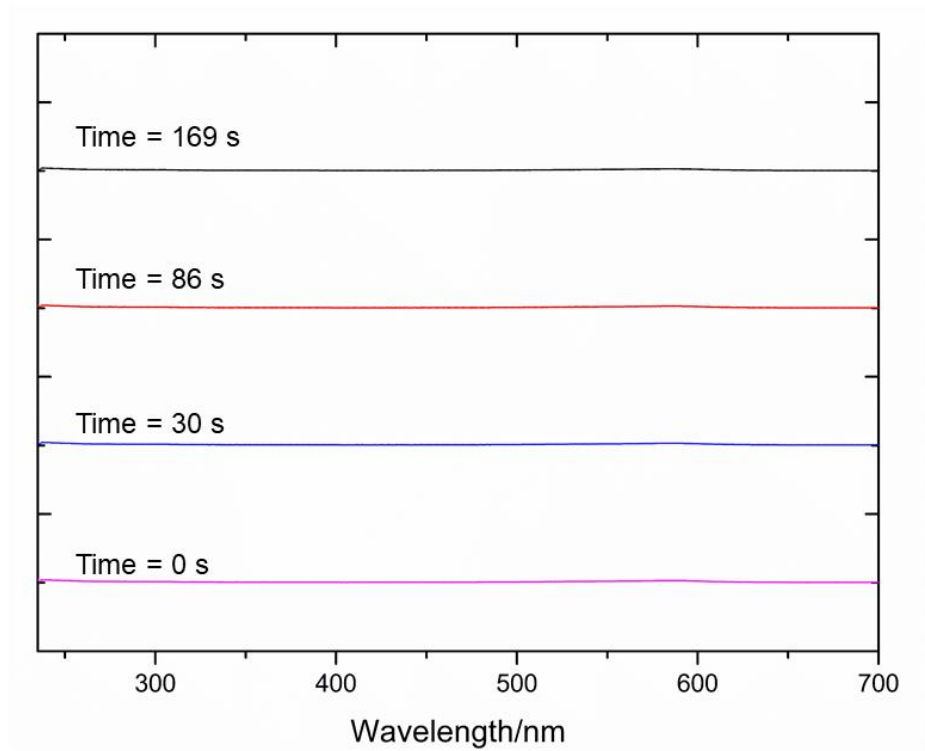


Figure S7. Time-dependent UV-vis spectra of F₁-SiG100's oil-water separation permeate.

A



B

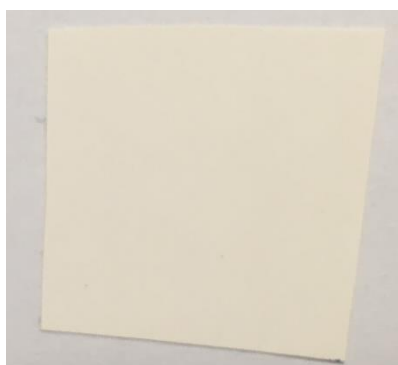


Figure S8. Photos of the (A) feed side holding the dyed water, and (B) the permeate side of the F₁-SiG100 membrane after oil-water separation testing.

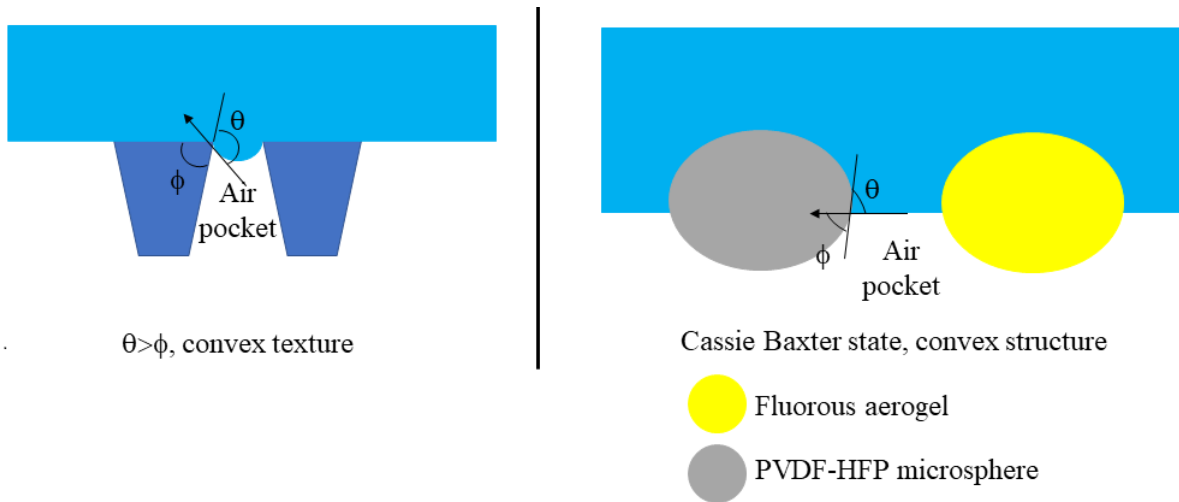


Figure S9. The re-entrant structures of the modified membranes.

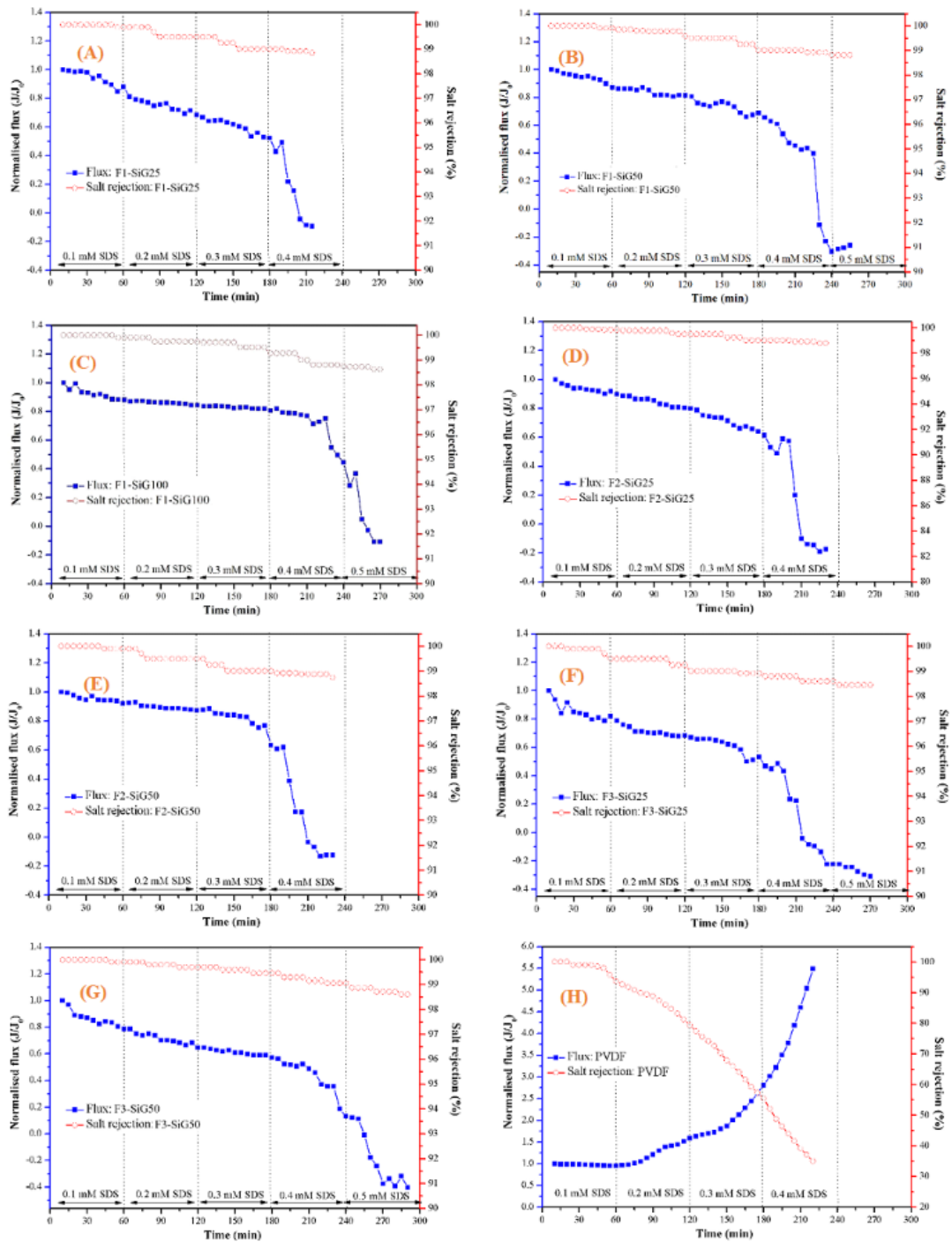


Figure S10. DCMD performances of the fluorinated aerogel membranes with stepwise SDS addition (0.1 ~ 0.5 mM) in 3.5% NaCl solution: (a) **F₁-SiG25**, (b) **F₁-SiG50**, (c) **F₁-SiG100**, (d) **F₂-SiG25**, (e) **F₂-SiG50**, (f) **F₃-SiG25**, (g) **F₃-SiG50**, and (h) C-PVDF membranes. The initial fluxes were observed as 24.29 ± 0.31 , 23.94 ± 0.52 , 24.25 ± 0.40 , 23.89 ± 0.27 , 24.12 ± 0.33 , 24.39 ± 0.51 , 23.76 ± 0.42 and 26.47 ± 0.47 L m⁻² h⁻¹, respectively

Table S1. Surface tension of solvents used in the study.

Solvents	Surface tension(σ_L) at room temperature /mN m ⁻¹	Dispersive component (σ_L^D) /mN m ⁻¹	Polar component (σ_L^P) /mN m ⁻¹
Water	72.8	21.8	51.0
Diiodomethane	50.8	50.8	0.0

Table S2. The BET surface area, porosity and surface free energy of membranes.

Type of membrane	BET surface area (m ² g ⁻¹)	Porosity (%)	Surface free energy (mN m ⁻¹)	Water contact angle (°)
F ₁ -SiG25	4.54	76.71 ± 0.56	2.16 ± 0.25	139.7±1.4
F ₁ -SiG50	5.34	78.18 ± 0.56	1.93 ± 0.27	141.5±2.0
F ₁ -SiG100	9.25	78.65 ± 0.60	0.82 ± 0.17	151.2±1.0
F ₂ -SiG25	9.85	75.01 ± 0.56	2.29 ± 0.23	138.0±1.0
F ₂ -SiG50	11.02	76.22 ± 0.45	1.89 ± 0.17	138.2±0.4
F ₃ -SiG25	10.14	73.69 ± 0.67	2.93 ± 0.49	131.6±2.6
F ₃ -SiG50	14.49	74.91 ± 0.65	1.99 ± 0.25	134.1±2.3
C-PVDF	3.60	64.11 ± 0.33	29.01 ± 0.71	119.0±3.1

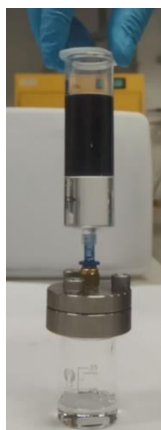
Table S3. Oil/water separation measurements and the oil adsorption of F₁-SiG100 membrane

	Absorption capacity (g g ⁻¹)	Flux (L m ⁻² h ⁻¹)
1 st	3.3	647.4
2 nd	3.0	687.9
3 rd	3.1	659.1
Average	3.2	664.8
Standard deviation	0.2	20.8

For oil//water separation, gravity driven based separation has been adopted, using chloroform (colourless) and water (dyed in blue colour).



At time 3 s



At time 30 s



At time 86 s



At time 169 s

Table S4. Comparison of DCMD performance against low surface tension feed.

Materials	Types	Feed concentration	Water flux/LMH	Duration	Feed temperature/°C	Permeate temperature/°C	Rejection
PDMS/aerogel/PVDF ¹	Electrospraying	3.5% wt% NaCl and 0.1 mM SDS	20	8 hours	60	20	99.99%
FTCS/PVDF ²	Electrospinning and dip-coating	3.5% wt% NaCl and 0.1 mM SDS	10	6 hours	60	20	99.99%
FAS17/PVDF-HFP ³	Electrospinning and dip coating	3.5% wt% NaCl and 0.1 mM SDS	19	2 hours	60	20	99.99%
PTFE-PVDF ⁴	Commercial (Minglie Membrane)	3.5% wt% NaCl and 0.3 mM SDS	11.8	50 hours	53	20	99.99%
FAS17/ZnO/glass fibers membrane ⁵	Polymer coating	1 M NaCl and 0.3 mM SDS	11.4	8 hours	60	20	99.99%
F ₁ -SiG100 (This study)	Electrospraying	3.5% wt% and 0.1 mM SDS	17.3	240 hours	60	20	99.99%

Method S1. Working principle, mathematical models and detailed procedure of measuring membranes surface roughness using optical surface profiler (Wyko NT9300, Veeco).

In optical surface profiler, the calculated average surface roughness, R_a , and the root mean square (RMS) roughness, R_{RMS} , are defined as the average height calculated over the entire measured length or area, and as the average between the height deviations and the mean surface taken over the evaluation area, respectively. R_a and R_{RMS} are calculated based on the (ANSI B46.1 2009) standard according to Equation (1) and Equation (2) below, respectively:

$$R_a = \frac{1}{MN} \sum_{j=1}^N \sum_{i=1}^M |Z_{ij}| \quad (\text{Equation 1})$$

$$R_{RMS} = \sqrt{\frac{1}{MN} \sum_{j=1}^N \sum_{i=1}^M Z^2(x_i, y_i)} \quad (\text{Equation 2})$$

Equations 1 and 2 apply for a three-dimensional measurement where M and N are the number of data points in X and Y, and Z is the surface height relative to the mean plane. The RMS roughness is representative of the standard deviation of the profile heights of the measured surface ⁶.

The working principle of surface profiling by White Light Interferometry (WLI) is shown in Figure 1 below, and can be briefly explained as follows:

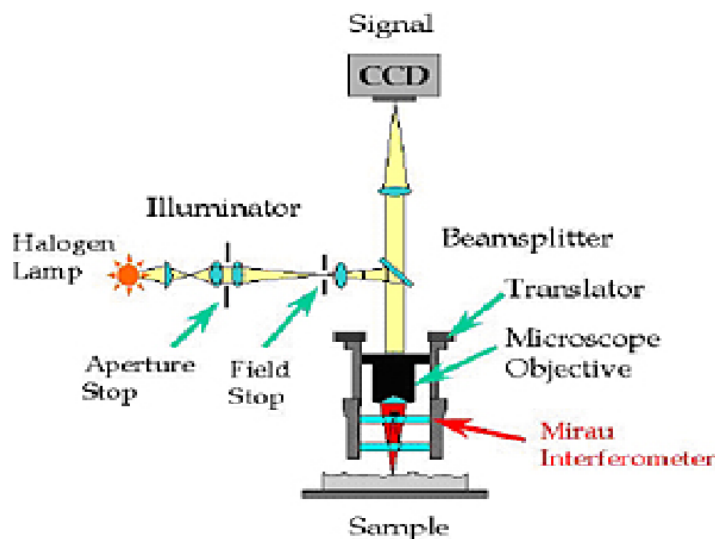


Figure 1. Typical microscope based white light interferometer⁷.

Firstly, a white light from the illuminator generated by a halogen lamp travels through the aperture stop and field stop. The aperture stop controls the light focus while the field stop controls the field-of-view (FOV) on the charged-coupled-device (CCD) camera. The light is then reflected down to the interferometer (interfaced with a translator, reference mirror, and a microscope objective) by a beam splitter. Once the light reaches the microscope objective, another beam splitter separates the light into two beams. One beam (the reference beam) reflects from a super smooth reference mirror inside the objective, while the other (the test beam) reflects from the surface of the sample and back to the objective. If the surface of the sample is in focus, the two light beams will recombine to create bright and dark bands called “fringes” that represent the topography of the object and can be used to gauge the roughness of the surface. Throughout the scan, a series of intensity of data frames, which are shown as interferograms, is recorded by the CCD detector and the data frame is forwarded to a computer for processing. Finally, these frames are analysed using various interferometric phase mapping programs, to determine the height of each point on the surface⁷.



Video S1. Superoliphilicity of F1-SiG100 by dropping chloroform.

https://portland-my.sharepoint.com/:v/g/personal/mwyim4-c_ad_cityu_edu_hk/EVVocMQPe6hCrVJNL1ER63ABBEpswtUMU7pnShLDT0XMkw?e=mfK3Ed

References

- 1 E.-J. Lee, B. J. Deka and A. K. An, *J. Memb. Sci.*, 2019, **573**, 570–578.
- 2 L. Deng, H. Ye, X. Li, P. Li, J. Zhang, X. Wang, M. Zhu and B. S. Hsiao, *Sep. Purif. Technol.*, 2018, **206**, 14–25.
- 3 X. An, Z. Liu and Y. Hu, *Desalination*, 2018, **432**, 23–31.
- 4 D. Hou, Z. Yuan, M. Tang, K. Wang and J. Wang, *J. Memb. Sci.*, 2020, **595**, 117495.
- 5 L. H. Chen, A. Huang, Y. R. Chen, C. H. Chen, C. C. Hsu, F. Y. Tsai and K. L. Tung, *Desalination*, 2018, **428**, 255–263.
- 6 S. E. Cross, J. Kreth, R. P. Wali, R. Sullivan, W. Shi and J. K. Gimzewski, *Dent. Mater.*, 2009, **5**, 1517–1526.
- 7 S. C. H. Thian, W. Feng, Y. S. Wong, J. Y. H. Fuh, H. T. Loh, K. H. Tee, Y. Tang and L. Lu, *J. Phys. Conf. Ser.*, 2007, **48**, 1435–1446.